Journal of Magnetism and Magnetic Materials 441 (2017) 417–423

Contents lists available at ScienceDirect

Journal of Magnetism and Magnetic Materials

journal homepage: www.elsevier.com/locate/jmmm

Research articles

Unusual variation of blocking temperature in bi-magnetic nanoparticles

Fernando Arteaga-Cardona [a,*], Esmeralda Santillán-Urquiza [b], Umapada Pal [c], M.E. Méndoza-Álvarez [c], Cristina Torres-Duarte [d], Gary N. Cherr [d,e], Patricia de la Presa [f,g], Miguel Á. Méndez-Rojas [a]

[a] Departamento de Ciencias Químico-Biológicas, Universidad de las Américas Puebla, ExHda. Sta. Catarina Martir s/n, San Andrés Cholula, 72810 Puebla, Mexico
[b] Departamento de Ingeniería Química, Alimentos y Ambiental, Universidad de las Américas Puebla, ExHda. Sta. Catarina Martir s/n, San Andrés Cholula, 72810 Puebla, Mexico
[c] Instituto de Física, Benemérita Universidad Autónoma de Puebla, Apdo. Postal J-48, Puebla, Pue. 72570, Mexico
[d] Bodega Marine Laboratory, UC-Davis, Bodega Bay, California, USA
[e] Department of Environmental Toxicology and Nutrition, UC-Davis, Davis, California, USA
[f] Instituto de Magnetismo Aplicado, UCM-ADIF-CSIC, Las Rozas, Spain
[g] Departamento de Física de Materiales, UCM, Ciudad Universitaria, Madrid, Spain

ARTICLE INFO

Article history:
Received 22 January 2017
Received in revised form 5 May 2017
Accepted 4 June 2017
Available online 5 June 2017

Keywords:
Blocking temperature
Ferrites
Bi-magnetic materials

ABSTRACT

Ferrite nanoparticles with bi-magnetic layered structure were synthesized by a seed-mediated co-precipitation technique. The strategy of growing a second magnetic layer enhanced the magnetic saturation (M_s) of the nanostructures, with a very small increase in their blocking temperature (T_B). In contrary to the common magnetic nanostructures of 10–15 nm size range, which manifest blocking temperatures around room temperature (≈300 K), the measured T_B values of the bi-magnetic nanostructures are much lower. The experimental T_B values of the bi-magnetic nanostructures are much lower than their theoretically predicted ones. Moreover, the T_B of the nanoparticles varies unusually, decreasing with particle size beyond a certain value. The low blocking temperature and high M_s of the fabricated bi-magnetic nanoparticles indicate the seed-mediated coprecipitation is an effective method for designing magnetic nanostructures suitable for biomedical applications such as in magnetic hyperthermia treatment, where nanostructures of low T_B and high M_s are required.

1. Introduction

Magnetic nanoparticles (MNPs) are attractive because of their many potential practical applications such as in magnetic storage, biomarkers, contrast agents, biomolecule separation, sensors, and for advanced clinical treatments [1–4]. In many of those applications; particularly for biomedical applications, it is desirable that the MNPs are superparamagnetic, to avoid aggregation in body fluid systems [3]. However, the MNPs often lose their superparamagnetic state and enter into a spin blocked regime even with sizes well-below of 20 nm. Although the critical size below which the MNPs remain superparamagnetic depends on their compositions, the dependence is not very significant [4–6]. Spin blocking occurs when the thermal energy (T_E) is less than the energy barrier (E_B) needed to produce the inversion of the spins ($E_B = K_{eff}V$). Since this E_B is proportional to the volume of the nanoparticles and the anisotropy of the spin-orbit coupling [7], increasing the size of nanoparticles increases the E_B [8,9]. That is the reason that most of the MNPs cannot be in a superparamagnetic regime above a certain size.

Many strategies have been utilized to control the blocking temperature (T_B) of magnetic nanomaterials. Most of them are based on the use of a diamagnetic material such as organic polymers and ceramic materials as a coating layer. The most common organic polymers used as coatings are polyols, dextran, oleic acid, carbohydrates chains, etc. [10–12]. These organic coatings also serve to stabilize the nanomaterials in suspension and induce additional functionalities to their surfaces. Common ceramic materials used as coatings for MNPs are SiO_2, $Ca_5(PO_4)_3OH$ and several other porous ceramic matrices [13–15]. Separation of disaggregation of MNPs reduces the anisotropy produced by interparticle interactions, i.e., dipole-dipole interactions. Since the energy of a magnetic dipole depends directly on its magnetic moment and inversely to the cubic distance between the poles ($E_D = \mu_0 * \mu^2/4\text{-}\pi d^3$) [9], this approach has given good results [14]. Although separating or disaggregating the MNPs helps to reduce their T_B, sometimes the use of a diamagnetic shell decreases the magnetic saturation (M_s) to less than 10 emu/g, due to the increase of non-magnetic mass.

* Corresponding author.
E-mail address: fernando.arteagaca@udlap.mx (F. Arteaga-Cardona).

http://dx.doi.org/10.1016/j.jmmm.2017.06.024
0304-8853/

Decreasing the M_s of MNPs may also reduce their efficiency in the desired applications. Often MNPs of high M_s are desired to improve their performance in hyperthermia treatments or as MRI contrast agents [16,17]. In hyperthermia treatment, the magnetic spins align with respect to an alternating magnetic field. So, the MNPs with high M_s values generate more friction and hence higher amount of heat [18]. On the other hand, in the use of MNPs as MRI contrast agent, high M_s values strongly affects the precession movement of hydrogen atoms [19]. An advantage of using a diamagnetic shell around/over MNPs is that it may lower the toxicity of the MNPs. The toxicity of some magnetic materials like ferrites, in particular, magnetite (Fe_3O_4), has been extensively studied [20–23] and most of the results reported no alteration in the normal behavior of the cells used to test the toxicity, suggesting good biocompatibility even at high doses. Contrast agents based on magnetite nanoparticles are also commercially available for clinical use.

It is difficult to compare the reported T_B values of MNPs due to the versatility of the conditions used to obtain their zero-field cooled (ZFC) curves, the synthesis procedure, the used coating materials, etc. However, for ferrites such as magnetite, the values are in the range of 10–280 K for nanoparticles of 4–14 nm size range. For cobalt ferrite ($CoFe_2O_4$), the common values are over 200 K, even for sizes around 4 nm, due to the high anisotropy of cobalt ions [24]. On the other hand, the reported T_B values for manganese ferrite ($MnFe_2O_4$) are very disperse. For the nanoparticles smaller than 10 nm, the reported values are often less than 150 K [25]. However, for nanoparticles larger than 12 nm, the value increases rapidly to more than 250 K [26]. Finally, the T_B values for reported core-shell structures like $MnFe_2O_4$@$CoFe_2O_4$ of 6–9 nm size range have been reported to vary between 130 and 270 K [27], and for CoO@$CoFe_2O_4$ nanoparticles of 5–11 nm size range, it varied from 167 to 388 K [28]. Although it is difficult to compare the reported T_B values of MNPs due to the reasons stated above, one thing remains clear, that for all the materials the T_B of MNPs always increases with their size.

Here, apart from reporting the fabrication of bi-magnetic $Zn_{0.5}Mn_{0.5}Fe_2O_4$@Fe_3O_4 core-shell nanoparticles of varied shell thickness, we discuss how these MNPs considerably increase their M_s with a minimum increase in their T_B. The T_B values obtained for these core-shell system does not follow any reported theory or model. After a certain optimum size, the T_B value even starts decreasing. Furthermore, *in vitro* assays (membrane integrity, production of reactive oxygen species (ROS), lysosomes abundance, cell viability, cell death, and zinc internalization) of the fabricated bi-magnetic nanoparticles have been carried out in mussel hemocytes to evaluate their potential cellular toxicity.

2. Materials and methods

All the chemicals were purchased from Sigma-Aldrich (Toluca, México). Manganese (II) chloride tetrahydrate ($MnCl_2{\cdot}4H_2O$, >98%), zinc chloride ($ZnCl_2$, >98%), sodium hydroxide (NaOH, >97%), iron (II) chloride tetrahydrate ($FeCl_2{\cdot}4H_2O$, >98%), iron (III) chloride hexahydrate ($FeCl_3{\cdot}6H_2O$, >97%), iron (III) nitrate nonahydrate ($Fe(NO_3)_3{\cdot}9H_2O$,>98%), hydrochloric acid (HCl, 37%) and nitric acid (HNO_3, 70%) were of reagent grade and used as received without further purification. Magnetic nanoparticles (MNPs) of zinc ferrite were obtained by co-precipitation as previously reported [29,30], followed by a seed-mediated synthesis to deposit a second magnetic layer [31].

2.1. Synthesis of zinc-manganese ferrite ($Zn_{0.5}Mn_{0.5}Fe_2O_4$) (ZnMn)

ZnMn nanoparticles were prepared by adding 1 mL of a solution of $ZnCl_2$ (1.25 μmol) and $MnCl_2{\cdot}4H_2O$ (1.25 μmol) into a 5 mL solution of $FeCl_3{\cdot}6H_2O$ (5 μmol) in water. The mixture was added to a 2 M solution of NaOH and stirred for 30 min at 100 °C. After 30 min stirring, the obtained black precipitate was washed three times with distilled water to remove excess precursor ions. The washed black precipitate was redispersed in water and used as seeds for the fabrication of bi-magnetic core-shell nanoparticles.

2.2. Synthesis of bi-magnetic core-shell ferrite MNPs ($Zn_{0.5}Mn_{0.5}Fe_2O_4$@Fe_3O_4) (ZnMn-Fet, t = 30 m, 1 h, 2 h, 3 h)

Previously prepared ZnMn MNPs were used as seeds for the growth of ZnMn@Fe_3O_4 core-shell structures. Briefly, a 6 mL solution of $FeCl_2{\cdot}4H_2O$ (2.5 μmol), $FeCl_3{\cdot}6H_2O$ (5 μmol) and 250 μL of HCl (37%) were added to the previously prepared ZnMn MNPs and left stirring for five minutes. Then, 40 mL of a 2 M NaOH solution was added to the mixture and stirred for 30 min (ZnMn-Fe30 m), 1 h (ZnMn-Fe1 h), 2 h (ZnMn-Fe2 h) and 3 h (ZnMn-Fe3 h) to grow magnetite layers of different thicknesses. After that time, the black precipitate was washed 3 times with distilled water to remove the unreacted precursor ions.

2.3. Water stabilization

Stabilization of the synthesized nanoparticles was achieved by acid peptization in aqueous media to reduce their potential aggregation [26,32]. In summary, 15 mL of HNO_3 (2 M) was added to the obtained ZnMn-Fet MNPs and stirred for 15 min. After that, the supernatant was magnetically decanted and 25 mL of a 1 M Fe $(NO_3)_3{\cdot}9H_2O$ solution was added and left stirring for 20 min at 100 °C. Finally, 15 mL of HNO_3 (2 M) were added under stirring. After 15 min, the supernatant was magnetically decanted and washed 2 times with acetone. The product was re-dispersed in water, obtaining a stable, water soluble ferrofluid.

3. Characterization

3.1. TEM, DLS and X-ray diffraction

Particle size and size dispersion of all the fabricated nanostructures were analyzed using a JEOL JEM1010 (JEOL USA, Inc., Peabody, MA) transmission electron microscope (Fig. S1, supplementary information). The hydrodynamic diameter of the samples was measured at room temperature using a NanoFlex dynamic light scattering (DLS) (Microtrac Inc., Montgomeryville, PA, USA) system, with a 780 nm wavelength laser of 3 mW power. X-ray diffraction (XRD) patterns of the samples were recorded using energy filtered Cu Kα radiation (λ = 1.5406 Å, Ni filter) in a PANalytical Empyrean diffractometer, between 15° and 80° of 2θ, at room temperature.

3.2. Magnetic measurements

Magnetic hysteresis and zero-field cooled (ZFC) curves were recorded in a Dynacool 9 physical property measurement system (PPMS, Dynacool 9, Quantum Design, USA) by placing the dry powder samples in tubular plastic sample holders. The hysteresis curves were recorded up to 5 T magnetic field at room temperature (≈300 K) and 10 K. ZFC curves were obtained by cooling the samples up to 10 K, without applying an external magnetic field; then a magnetic field of 100 Oe was applied and heating started at a rate of approximately 0.02 K/s until a temperature of 300 K was reached.

3.3. Toxicity assays

For the potential toxicology evaluation of the nanostructures, mussel hemocytes cells were used. Hemocytes are the cells of the immune system of mussels, that have been extensively used in the nanotoxicological analysis. Multiple parameters of cell toxicity were evaluated including mitochondrial membrane damage, production of reactive oxygen species (ROS), cell viability, cell death and lysosome abundance, as well as soluble zinc uptake. The effects of ZnMn, ZnMn-Fe1 h, and ZnMn-Fe3 h were evaluated as representative samples. The complete description of the toxicity evaluation of the samples by this model is available in the SI section.

4. Results and discussion

4.1. Size and crystallographic results

The average size of the MNPs used as seeds (ZnMn) determined by TEM was around 8.0 ± 0.2 nm, while for the core-shell structures, the size increased to 10.0 ± 0.3, 11.5 ± 0.2, 12.3 ± 0.2 and 13.0 ± 0.3 nm for the reactions of 30 min, 1 h, 2 h and 3 h, respectively. These values were calculated by the average of more than 300 well-defined nanoparticles at different areas. The size increase of the second layer with reaction time agreed with previous reports for seed-mediated synthesis [28,33,34]. Discussion of the DLS analysis of the aqueous colloids can be found at the SI [35].

X-ray diffraction patterns of the samples revealed typical spinel structure of ferrites (Fig. S2, supplementary information). The XRD pattern of the Fe_3O_4 coated bi-magnetic NPs looks noisy with respect to the obtained pattern of the ZnMn nanoparticles. The noise could be attributed to a disordered layer of Fe_3O_4 [29].

4.2. Magnetometry measurements

Magnetization curves of the samples recorded at 300 K (Fig. 1a) show an increase in M_s for bi-magnetic structures, as compared to the core ZnMn MNPs. The M_s of the ZnMn ferrite is about 42 emu/g, while for ZnMn-Fe30 m it is about 49 emu/g (16% increase). For ZnMn-Fe1 h, M_s increases to 56 emu/g (33% increase). For ZnMn-Fe2 h and ZnMn-Fe3 h, the M_s values were 53 and 52 emu/g, respectively, which are higher than the values obtained for ZnMn and ZnMn-Fe30 m, but lower than the M_s value of ZnMn-Fe1 h. This decrease might be associated to the mass ratio between ZnMn and Fe_3O_4 in the bi-magnetic system. If the mass fraction of ZnMn is considerably higher than the mass fraction of Fe_3O_4, then the magnetic properties of the bi-magnetic nanoparticles should be more like the ZnMn core. However, if more Fe_3O_4 is present, then the magnetic contribution of Fe_3O_4 to the total magnetization should be higher. The results presented above indicate that there is a limit on the thickness of the second magnetic layer, up to which M_s increases. Below and above that limit, the contribution of one of the components (core or the shell) becomes greater than the other one. Thus, the whole system starts to behave more like the component (material) more abundant.

Although all the M_s values of the bi-magnetic Fe_3O_4 coated MNPs were significantly greater than the values of the ZnMn nanoparticles at 300 K, the determined M_s at 10 K (Fig. 1b) show considerable differences. At 10 K, the sample with highest M_s was ZnMn-Fe1 h, with a value of 82 emu/g, which was also the sample with the largest M_s at 300 K. However, ZnMn had the second largest M_s value at 10 K (77 emu/g), followed by ZnMn-Fe30 m with a M_s of 74 emu/g. Finally, ZnMn-Fe2 h and ZnMn-Fe3 h presented the lower values with M_s of 73 and 70 emu/g, respectively.

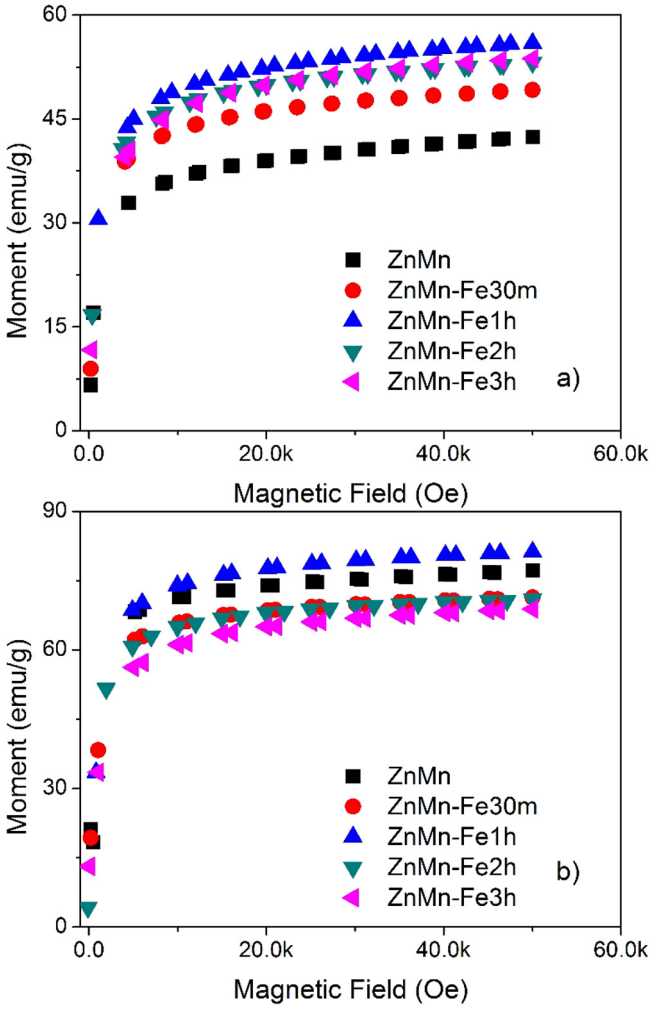

Fig. 1. Magnetization curves for the bi-magnetic nanostructures at a) 300 K, and b) 10 K.

These results appear incoherent since the samples with lower M_s values at 300 K had the second and third largest values at 10 K. However, the XRD patterns of the core-shell structures suggest that the Fe_3O_4 shell layers have different crystallographic orientations than the ZnMn core. At temperatures around 300 K, the thermal energy should be enough to overcome the E_B [36], and the spins of the Fe_3O_4 layer can align with the magnetic field increasing the M_s value. However, at low temperatures (e.g. 10 K), the thermal energy is not enough to overcome the E_B, and the Fe_3O_4 spins remain randomly oriented [37], reducing the M_s value of the entire structure.

A close-up of the remanent magnetization area in the hysteresis loops is presented in Fig. 2. It can be seen that at room temperature (Fig. 2a), the samples have negligible coercivity (H_c < 50 Oe), suggesting superparamagnetism below 300 K with low anisotropy. However, at 10 K (Fig. 2b), the hysteresis loops are wider, although the H_c remained low (H_c < 300 Oe).

4.3. Blocking temperature determination

The T_B values for all the MNPs were determined from the maximum of their ZFC curves [38–41] obtained for a 100 Oe applied field. The maximum of ZFC curves can be used to determine the T_B because the samples were cooled in absence of any magnetic field, and then a small magnetic field was applied to measure the

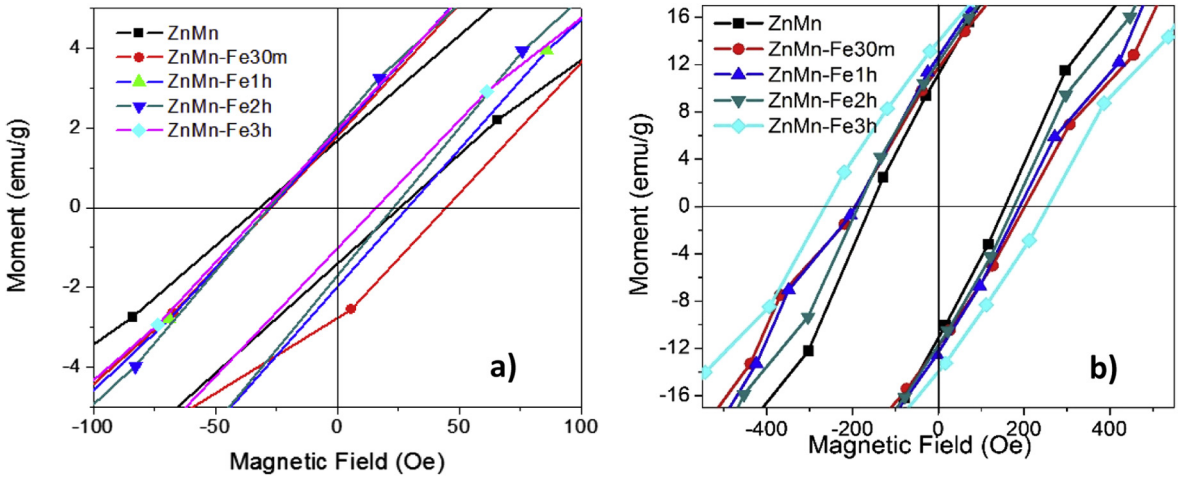

Fig. 2. Amplified low-field sections of the hysteresis loops of the samples showing their coercivity at a) 300 K and at b) 10 K.

polarization of their spins aligned to the magnetic field [42]. On slowly increasing the temperature, the thermal energy increases, and the spins of the MNPs, which have a low E_B, get aligned in parallel to the applied magnetic field. The unaligned spins also get aligned later at higher thermal energy, increasing the magnetization until the point where most of the spins are unblocked, and that is when the ZFC curve reaches its maximum. By increasing further the temperature, the thermal energy also increases and it may become high enough to slightly misalign the spins with respect to the magnetic field, inducing a decrease on the magnetization [43,44].

Fig. 3 shows the ZFC curves for all the MNPs fabricated in this work. The sample with lowest T_B is ZnMn ($T_B \approx 100$ K), which was used as seed particles for fabricating core-shell nanostructures. All the bi-magnetic nanoparticles revealed higher T_B, depending on their shell thickness. The increase of T_B in bi-magnetic core-shell structures might be due to: a) their bigger sizes, and b) magnetic anisotropy (K_{eff}) between the core and the shell layers. Although the T_B of all the core-shell bi-magnetic nanoparticles increased to some extent, the ZnMn-Fe1 h sample revealed highest T_B, which is around 150 K. However, the value is considerably lower than the previously reported T_B values for any magnetic nanoparticle larger than 10 nm.

Although the T_B of the MNPs suffered only a slight increase after the formation of Fe_3O_4 shell layer, their M_s values increased significantly (inset of Fig. 4). Such low T_B and high M_s values of the bi-magnetic nanoparticles make them very attractive for biomedical applications such as in magnetic hyperthermia, where superparamagnetic nanostructures of low T_B with high M_s values are required [45].

4.4. Comparison of the experimental values with calculated T_B values obtained from the blocking temperature formula

To compare the results of our bi-magnetic nanostructures with previously reported models, we calculated their T_B by using the Eq. (1) [43]:

$$T_B = \frac{VK_{eff}}{k_B \ln(\tau_m/\tau_0)} \quad (1)$$

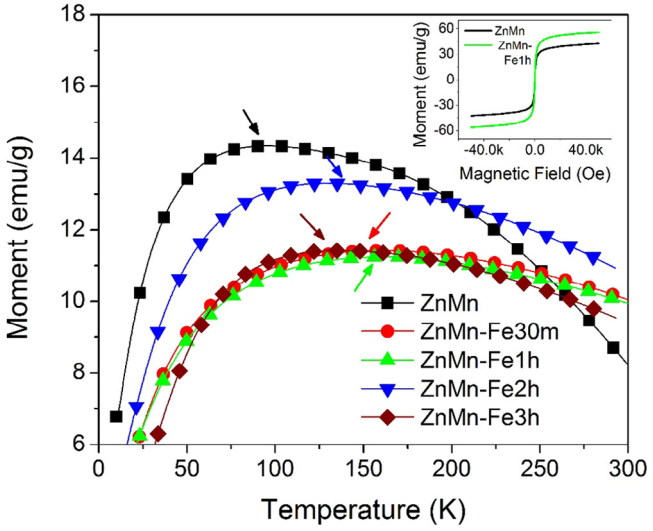

Fig. 3. ZFC curves of the MNPs used to estimate their T_B, arrows show the blocking temperature measured. The inset shows the hysteresis curves of ZnMn (black line) and ZnMn-Fe1 h (green line) recorded at 300 K. (For interpretation of the references to colour in this figure legend, the reader is referred to the web version of this article.)

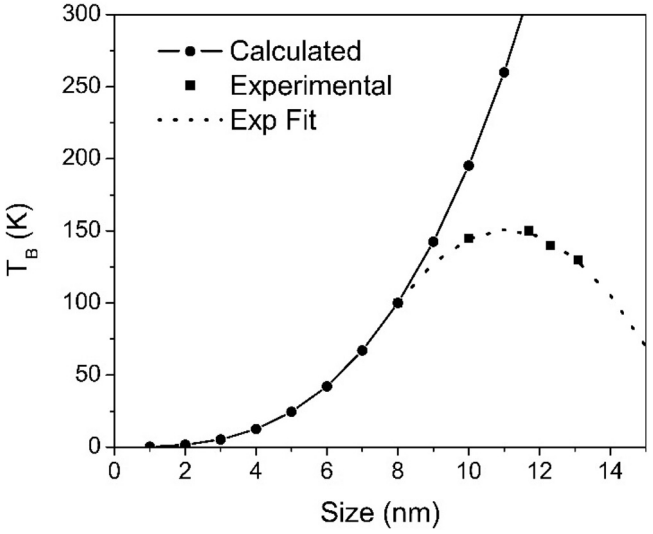

Fig. 4. Variation of calculated (filled circular data points connected with a continuous line) and experimental (square points connected with a dotted line) T_B values for MNPs with particle size.

where k_B is the Boltzmann constant (1.38×10^{-23} J/K), τ_0 the attempt time (with a value between 10^{-9} and 10^{-12} s), and τ_m the time of the measurement, which is the inverse of the measurement frequency. T_B is strongly dependent of the frequency, because if the spin changes its direction during the time window of the measurement, the material should appear as superparamagnetic, while in the case that the spin does not change its direction at the time window, the material would appear as blocked [46].

To obtain the relationship between the size and blocking temperature of the MNPs, first we estimated the K_{eff} of ZnMn MNPs from Eq. (1), utilizing their experimentally obtained volume and T_B values. The calculated value of the logarithmic function in the denominator of Eq. (1) ($\ln \tau_m/\tau_0$) was 25.16, which agrees with the commonly reported values around 25 [39,47]. By keeping the calculated K_{eff} value of ZnMn MNPs fixed, we varied the volume (V) of the nanoparticles from 1 to 14 nm to obtain their T_B for different sizes (Fig. 4). As can be seen from Fig. 4, MNPs of 12–14 nm size range should have a T_B close to 300 K (continuous line) if they follow the T_B equation (Eq. (1)), agreeing with most of the reported T_B values. However, the estimated T_B values of the bi-metallic MNPs fabricated in this work (plotted in Fig. 5 with squares and dotted line) do not follow the same trend, indicating a clear disagreement with calculations.

Although the increasing trend of T_B was followed up to a certain particle size, the trend is opposite after a critical size. This decreasing trend of T_B for bigger MNPs is probably due to the higher mass fraction of Fe_3O_4 in the bi-magnetic particles. The Fe_3O_4 layer, on its own, should have a lower T_B value than that of ZnMn particles. Increasing the size or the thickness of the Fe_3O_4 layer diminishes the magnetic properties of the whole nanostructure such as its M_s (as shown in Fig. 1) and T_B, as it measures the average properties of the whole system.

To compare our results with their reported values, some reported values of the blocking temperature for different ferrites are plotted in Fig. 5 in comparison with our calculated and experimental T_B values. As can be noticed, most of the reported T_B values remain close to the calculated line, but some of them are even higher than their theoretical (calculated) values. Such differences might be due to the variation of conditions used for the experiments (sample preparation and characterization). In addition, all the values reported for MNPs larger than 12 nm are blocked near room temperature, whereas, the T_B of our MNPs of similar sizes are well below the room temperature.

4.5. Simulation of ZFC curves

To visualize the unusual magnetic behavior of our bi-magnetic MNPs clearly, we simulated their ZFC curves theoretically by using a simple analytical zeroth order approximation (M^0_{ZFC}) described by Tournus and coworkers using the Eq. (2) [39,47]:

$$M^0_{ZFC} = M_B e^{-\tau\delta t} + M_{Eq}(1 - e^{-\tau\delta t}) \quad (2)$$

where τ corresponds to the Néel relaxation ($\tau = \tau_0 \exp(E_B/k_BT)$), and $\delta t = k_BT^2/vE_B$; M_B represents the blocked part ($M_B = \mu_0\mu H/3E_B$) and M_{Eq} the part at equilibrium ($M_{Eq} = \mu_0\mu H/3k_BT$), both depending on the vacuum permeability (μ_0) and the magnetic moment (μ), which can be calculated from the M_s and particle volume ($\mu = VM_s$). The particle volume V was calculated from TEM results, assuming a spherical shape of the MNPs. The calculated ZFC curves are presented in Fig. 6. The magnetization values of the curves were normalized for better visualization of the shifts of the maxima of ZFC curves, i.e. between the T_B values of the MNPs.

The results shown in Fig. 6 are in agreement with the calculated T_B values presented in Fig. 4, where MNPs with a size around 13 nm are often in the blocked state at room temperature. However, the T_B values obtained from the zeroth order expression still remains very different from the experimental T_B values, as the experimental values are much lower than the calculations and present an unusual variation, which is a decrease for the largest size MNPs.

A possible explanation of the vast differences between the experimental and theoretical T_B values can be attributed to the complexity of the layered structure of the MNPs. Probably, the Fe_3O_4 shell layers do not modify the size-related influence on the magnetic properties of ZnMn nanoparticles used as cores, as the Fe_3O_4 layer may just interact by a weak coupling. This coupling is the result of the different magnetic properties of the Fe_3O_4 shell with respect to the magnetic properties of ZnMn, such as lower M_s. Therefore, the small changes in the experimental T_B values among the samples might only be through the contribution of anisotropy by dipolar interactions or a spin-orbit coupling between the layers. The shifts associated to anisotropy can be described by Eq. (3) [2]:

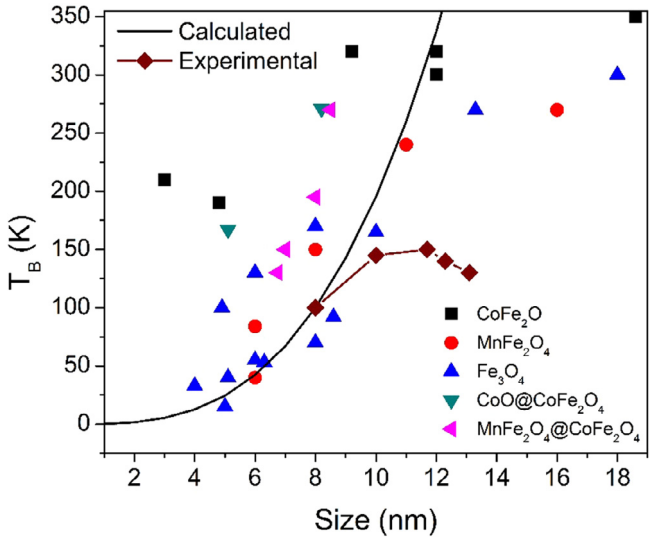

Fig. 5. Reported T_B values for different ferrites (different colored shapes), in comparison with the calculated values (continuous line) and our experimentally obtained values (brown rhombus). The values are taken from references [12,24–26,28,33,40,48–56]. (For interpretation of the references to colour in this figure legend, the reader is referred to the web version of this article.)

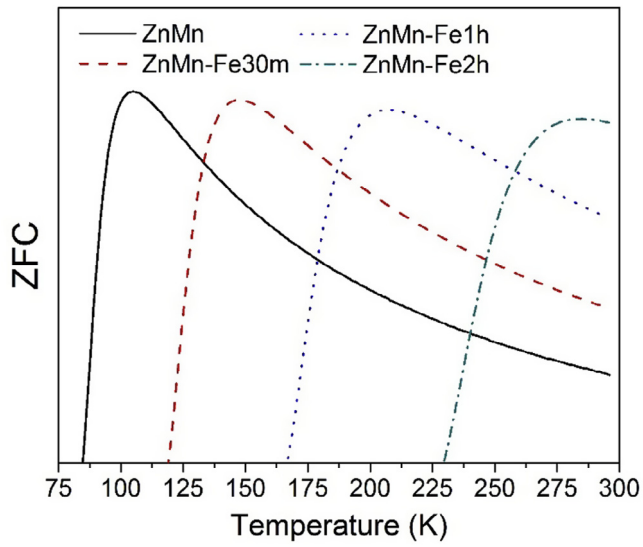

Fig. 6. Calculated ZFC curves for the MNPs, obtained from a zeroth order approximation expression.

$$K = K_i + \frac{6K_e}{D} \quad (3)$$

where K_i represents the anisotropy constant of the internal layer, in this case, the ZnMn; K_e represents the contribution of the anisotropy of the external magnetic layer (Fe_3O_4), and D represents the diameter of the MNPs.

As has been stated before, the main use of these bi-magnetic MNPs with low and tunable T_B might be in biomedicine. Therefore, we performed their toxicity tests in mussel hemocytes. Several parameters such as membrane integrity, ROS production, cell death or lysosome abundance and viability were evaluated. The results are presented in supporting information. The results indicate that only the viability of the hemocytes decreases for MNPs concentrations above 20 ppm. All the other tests turned out positive. These results indicate that the MNPs fabricated in this work could be utilized for biomedical applications.

5. Conclusion

Bi-magnetic zinc-manganese ferrite nanoparticles coated with Fe_3O_4 were successfully prepared and characterized. The magnetite shell layer enhances the M_s of the bi-magnetic nanostructures. Although the size of the ferrite nanoparticles increases due to the formation of the Fe_3O_4 layer around them, their T_B barely changes in comparison to the reported values, where MNPs with an average size larger than 13 nm are almost blocked at a room temperature. The experimental values of T_B of our bi-magnetic nanoparticles were compared to those obtained from two different theoretical models and reported values, showing that the bi-magnetic nanostructures present an unusual variation of their T_B. The design and synthesis strategies used to fabricate bi-magnetic nanoparticles in this work can be utilized for precise tailoring of magnetic properties of nanomaterials. The toxicology tests carried out over mussels hemocytes model revealed the bi-magnetic nanoparticles have no substantial toxicity for such cells. Further studies are in progress to understand the relationship between the concentration of the core, concentration of the magnetite shell layer, and the magnetic properties of the core@shell structures.

Acknowledgments

This work was partially funded by UC-MEXUS/CONACYT Collaborative Research Program (Grant # CN-15-1472), and CONACYT, Mexico (Grant # INFR-2014-02-23053).

Appendix A. Supplementary data

Supplementary data associated with this article can be found, in the online version, at http://dx.doi.org/10.1016/j.jmmm.2017.06.024.

References

[1] J.G.S. Deb, D. Datta, D. Bahadur, Synthesis and characterization of biocompatible hydroxyapatite-coated ferrite, Bull. Mater. Sci. 26 (2003) 655–660, http://dx.doi.org/10.1007/BF02706759.
[2] G.C. Papaefthymiou, Nanoparticle magnetism, Nano Today 4 (2009) 438–447, http://dx.doi.org/10.1016/j.nantod.2009.08.006.
[3] Q.T. Bui, Q.A. Pankhurst, K. Zulqarnain, Inter-particle interactions in biocompatible magnetic fluids, Magn. IEEE Trans. 34 (1998) 2117–2119, http://dx.doi.org/10.1109/20.706822.
[4] W. Wei, W. Zhaohui, Y. Taekyung, J. Changzhong, K. Woo-Sik, Recent progress on magnetic iron oxide nanoparticles: synthesis, surface functional strategies and biomedical applications, Sci. Technol. Adv. Mater. 16 (2015) 23501, http://dx.doi.org/10.1088/1468-6996/16/2/023501.
[5] O.M. Lemine, K. Omri, M. Iglesias, V. Velasco, P. Crespo, P. de la Presa, L. El Mir, H. Bouzid, A. Yousif, A. Al-Hajry, γ-Fe_2O_3 by sol–gel with large nanoparticles size for magnetic hyperthermia application, J. Alloys Compd. 607 (2014) 125–131, http://dx.doi.org/10.1016/j.jallcom.2014.04.002.
[6] M. Veverka, K. Závěta, O. Kaman, P. Veverka, K. Knížek, E. Pollert, M. Burian, P. Kašpar, Magnetic heating by silica-coated Co–Zn ferrite particles, J. Phys. D Appl. Phys. 47 (2014) 65503, http://dx.doi.org/10.1088/0022-3727/47/6/065503.
[7] C. Ostenfeld, S. Mørup, Magnetic Interactions between nanoparticles of different materials, Hyperfine Interact. (2002) 83–86, http://dx.doi.org/10.1007/978-94-010-0281-3_21.
[8] P. Crespo, P. de la Presa, P. Marín, M. Multigner, J.M. Alonso, G. Rivero, F. Yndurain, J.M. González Calbet, A. Hernando, Magnetism in nanoparticles: tuning properties with coatings, J. Phys. Condens. Matter. 25 (2013) 484006, http://dx.doi.org/10.1088/0953-8984/25/48/484006.
[9] S. Mørup, M.F. Hansen, C. Frandsen, Magnetic interactions between nanoparticles, Beilstein J. Nanotechnol. 1 (2010) 182–190, http://dx.doi.org/10.3762/bjnano.1.22.
[10] F. Arteaga-Cardona, E. Gutiérrez-García, S. Hidalgo-Tobón, C. López-Vasquez, Y. A. Brito-Barrera, J. Flores-Tochihuitl, A. Angulo-Molina, J.R. Reyes-Leyva, R. González-Rodríguez, J.L. Coffer, U. Pal, M.P.-P. Diaz-Conti, D. Platas-Neri, P. Dies-Suarez, R.S. Fonseca, O. Arias-Carrión, M.A. Méndez-Rojas, Cell viability and MRI performance of highly efficient polyol-coated magnetic nanoparticles, J. Nanoparticle Res. 18 (2016) 345, http://dx.doi.org/10.1007/s11051-016-3646-0.
[11] E. Santillán-Urquiza, F. Arteaga-Cardona, E. Hernandez-Herman, P.F. Pacheco-García, R. González-Rodríguez, J.L. Coffer, M.E. Mendoza-Alvarez, J.F. Vélez-Ruiz, M.A. Méndez-Rojas, Inulin as a novel biocompatible coating: evaluation of surface affinities toward $CaHPO_4$, α-Fe_2O_3, ZnO, $CaHPO_4$@ZnO and α-Fe_2O_3@ZnO nanoparticles, J Colloid Interface Sci. 460 (2015) 339–348, http://dx.doi.org/10.1016/j.jcis.2015.08.057.
[12] R. Scholz, P. Wust, H. Schirra, T. Schiestel, R. Felix, Endocytosis of dextran and silan-coated magnetite nanoparticles and the effect of intracellular hyperthermia on human mammary carcinoma cells in vitro, J. Magn. Magn. Mater. 194 (1999) 185–196, http://dx.doi.org/10.1016/S0304-8853(98)00558-7.
[13] G.F. Goya, M.P. Morales, Field dependence of blocking temperature in magnetite nanoparticles, J. Metastable Nanocryst. Mater. 20–21 (2004) 673–678, http://dx.doi.org/10.4028/www.scientific.net/JMNM.20-21.673.
[14] K. Rumpf, P. Granitzer, P.M. Morales, P. Poelt, M. Reissner, Variable blocking temperature of a porous silicon/Fe_3O_4 composite due to different interactions of the magnetic nanoparticles, Nanoscale Res. Lett. 7 (2012) 445–448, http://dx.doi.org/10.1186/1556-276X-7-445.
[15] H.-M. Song, J.I. Zink, N.M. Khashab, Seeded growth of ferrite nanoparticles from Mn oxides: observation of anomalies in magnetic transitions, Phys. Chem. Chem. Phys. 17 (2015) 18825–18833, http://dx.doi.org/10.1039/C5CP01301A.
[16] F. Arteaga-Cardona, S. Hidalgo-Tobón, U. Pal, M.Á. Méndez-Rojas, Ferrites as magnetic fluids for hyperthermia and MRI contrast agents, AIP Conf. Proc. 1747 (2016), http://dx.doi.org/10.1063/1.4954118.
[17] A. Lopez-Ortega, M. Estrader, G. Salazar-Alvarez, A.G. Roca, J. Nogues, Applications of exchange coupled bi-magnetic hard/soft and soft/hard magnetic core/shell nanoparticles, Phys. Rep. Rev. Sect. Phys. Lett. 553 (2015) 1–32, http://dx.doi.org/10.1016/J.Physrep. 2014.09.007.
[18] C.L. Dennis, R. Ivkov, Physics of heat generation using magnetic nanoparticles for hyperthermia, Int. J. Hyperth. 29 (2013) 715–729, http://dx.doi.org/10.3109/02656736.2013.836758.
[19] H. Shokrollahi, Contrast agents for MRI, Mater. Sci. Eng. C Mater. Biol. Appl. 33 (2013) 4485–4497, http://dx.doi.org/10.1016/j.msec.2013.07.012.
[20] R. Gabbasov, V. Cherepanov, M. Chuev, M. Polikarpov, M. Nikitin, S. Deyev, V. Panchenko, Biodegradation of magnetic nanoparticles in mouse liver from combined analysis of mössbauer and magnetization data, IEEE Trans. Magn. 49 (2013) 394–397, http://dx.doi.org/10.1109/TMAG.2012.2226148.
[21] M. Kawanishi, S. Ogo, M. Ikemoto, Y. Totsuka, K. Ishino, K. Wakabayashi, T. Yagi, Genotoxicity and reactive oxygen species production induced by magnetite nanoparticles in mammalian cells, J. Toxicol. Sci. 38 (2013) 503–511, http://dx.doi.org/10.2131/jts.38.503.
[22] M. Mesarosova, K. Kozics, A. Babelova, E. Regendova, M. Pastorek, D. Vnukova, B. Buliakova, F. Razga, A. Gabelova, The role of reactive oxygen species in the genotoxicity of surface-modified magnetite nanoparticles, Toxicol Lett. 226 (2014) 303–313, http://dx.doi.org/10.1016/j.toxlet.2014.02.025.
[23] A. Angulo-Molina, M.Á. Méndez-Rojas, T. Palacios-Hernández, O.E. Contreras-López, G.A. Hirata-Flores, J.C. Flores-Alonso, S. Merino-Contreras, O. Valenzuela, J. Hernández, J. Reyes-Leyva, Magnetite nanoparticles functionalized with α-tocopheryl succinate (α-TOS) promote selective cervical cancer cell death, J. Nanoparticle Res. 16 (2014) 1–12, http://dx.doi.org/10.1007/s11051-014-2528-6.
[24] Y. Il Kim, D. Kim, C.S. Lee, Synthesis and characterization of $CoFe_2O_4$ magnetic nanoparticles prepared by temperature-controlled coprecipitation method, Phys. B Condens. Matter. 337 (2003) 42–51, http://dx.doi.org/10.1016/s0921-4526(03)00322-3.
[25] S. Gubbala, H. Nathani, K. Koizol, R.D.K. Misra, Magnetic properties of nanocrystalline Ni – Zn, Zn – Mn, and Ni – Mn ferrites synthesized by reverse micelle technique, Phys. B Condens. Matter. 348 (2004) 317–328, http://dx.doi.org/10.1016/j.physb.2003.12.017.
[26] F. Arteaga-Cardona, K. Rojas-Rojas, R. Costo, M.A. Mendez-Rojas, A. Hernando, P. de la Presa, Improving the magnetic heating by disaggregating nanoparticles, J. Alloys Compd. 663 (2016) 636–644, http://dx.doi.org/10.1016/j.jallcom.2015.10.285.
[27] Q. Song, Z.J. Zhang, Controlled synthesis and magnetic properties of bimagnetic spinel, J. Am. Chem. Soc. 134 (2012) 10182–10190, http://dx.doi.org/10.1021/ja302856z.

[28] G.C. Lavorato, E. Lima, D. Tobia, D. Fiorani, H.E. Troiani, R.D. Zysler, E.L. Winkler, Size effects in bimagnetic CoO/$CoFe_2O_4$ core/shell nanoparticles, Nanotechnology 25 (2014), http://dx.doi.org/10.1088/0957-4484/25/35/355704.
[29] F. Arteaga-Cardona, E. Santillán-Urquiza, P. de la Presa, S.H. Tobón, U. Pal, P. Horta-Fraijo, M. José-Yacaman, J.D. Lozada Ramírez, R. Ivkov, A. Angulo-Molina, M.Á. Méndez-Rojas, Enhanced magnetic properties and MRI performance of bi-magnetic core–shell nanoparticles, RSC Adv. 6 (2016) 77558–77568, http://dx.doi.org/10.1039/C6RA14265F.
[30] R. Massart, Preparation of aqueous magnetic liquids in alkaline and acidic media, Magn. IEEE Trans. 17 (1981) 1247–1248, http://dx.doi.org/10.1109/TMAG.1981.1061188.
[31] N.T.K. Thanh, N. Maclean, S. Mahiddine, Mechanisms of nucleation and growth of nanoparticles in solution, Chem. Rev. 114 (2014) 7610–7630, http://dx.doi.org/10.1021/cr400544s.
[32] E. Auzans, D. Zins, E. Blums, R. Massart, Synthesis and properties of Mn-Zn ferrite ferrofluids, J. Mater. Sci. 34 (1999) 1253–1260, http://dx.doi.org/10.1023/A:1004525410324.
[33] J. Mohapatra, A. Mitra, D. Bahadur, M. Aslam, Surface controlled synthesis of MFe2O4 (M = Mn, Fe Co, Ni and Zn) nanoparticles and their magnetic characteristics, CrystEngComm. 15 (2013) 524–532, http://dx.doi.org/10.1039/C2CE25957E.
[34] C.S.S.R. Kumar, Magnetic Nanomaterials, Wiley, 2009.
[35] J. Lim, S.P. Yeap, H.X. Che, S.C. Low, Characterization of magnetic nanoparticle by dynamic light scattering, Nanoscale Res. Lett. 8 (2013), http://dx.doi.org/10.1186/1556-276X-8-381.
[36] B. Issa, I.M. Obaidat, B.A. Albiss, Y. Haik, Magnetic nanoparticles: Surface effects and properties related to biomedicine applications, Int. J. Mol. Sci. 14 (2013) 21266–21305, http://dx.doi.org/10.3390/ijms141121266.
[37] A.E. Berkowitz, R.H. Kodama, S.A. Makhlouf, F.T. Parker, F.E. Spada, E.J. McNiff Jr., S. Foner, Anomalous properties of magnetic nanoparticles, J. Magn. Magn. Mater. 196–197 (1999) 591–594, http://dx.doi.org/10.1016/S0304-8853(98)00845-2.
[38] R.K. Zheng, G. Hongwei, X. Bing, X.X. Zhang, The origin of the non-monotonic field dependence of the blocking temperature in magnetic nanoparticles, J. Phys. Condens. Matter. 18 (2006) 5905, http://dx.doi.org/10.1088/0953-8984/18/26/010.
[39] F. Tournus, E. Bonet, Magnetic susceptibility curves of a nanoparticle assembly, I: theoretical model and analytical expressions for a single magnetic anisotropy energy, J. Magn. Magn. Mater. 323 (2011) 1109–1117, http://dx.doi.org/10.1016/j.jmmm.2010.11.056.
[40] P. de la Presa, Y. Luengo, M. Multigner, R. Costo, M.P. Morales, G. Rivero, A. Hernando, Study of heating efficiency as a function of concentration, size, and applied field in γ-Fe_2O_3nanoparticles, J. Phys. Chem. C. 116 (2012) 25602–25610, http://dx.doi.org/10.1021/jp310771p.
[41] A. Kolhatkar, A. Jamison, D. Litvinov, R. Willson, T. Lee, Tuning the magnetic properties of nanoparticles, Int. J. Mol. Sci. 14 (2013) 15977, http://dx.doi.org/10.3390/ijms140815977.
[42] J. García-Otero, M. Porto, J. Rivas, A. Bunde, Influence of dipolar interaction on magnetic properties of ultrafine ferromagnetic particles, Phys. Rev. Lett. 84 (2000) 167–170, http://dx.doi.org/10.1103/PhysRevLett. 84.167.
[43] M.S. Seehra, K.L. Pisane, Relationship between blocking temperature and strength of interparticle interaction in magnetic nanoparticle systems, J. Phys. Chem. Solids. 93 (2016) 79–81, http://dx.doi.org/10.1016/j.jpcs.2016.02.009.
[44] V. Russier, Blocking temperature of interacting magnetic nanoparticles with uniaxial and cubic anisotropies from Monte Carlo simulations, J. Magn. Magn. Mater. 409 (2016) 50–55, http://dx.doi.org/10.1016/j.jmmm.2016.02.070.
[45] K. Simeonidis, C. Martinez-Boubeta, L. Balcells, C. Monty, G. Stavropoulos, M. Mitrakas, A. Matsakidou, G. Vourlias, M. Angelakeris, Fe-based nanoparticles as tunable magnetic particle hyperthermia agents, J. Appl. Phys. 114 (2013) 103904, http://dx.doi.org/10.1063/1.4821020.
[46] A.A. Timopheev, V.M. Kalita, S.M. Ryabchenko, Simulation of the magnetization reversal of an ensemble of single-domain particles in measurements with a continuous sweep of the magnetic field or temperature, Low Temp. Phys. 34 (2008) 446–457, http://dx.doi.org/10.1063/1.2920171.
[47] F. Tournus, A. Tamion, Magnetic susceptibility curves of a nanoparticle assembly II. Simulation and analysis of ZFC/FC curves in the case of a magnetic anisotropy energy distribution, J. Magn. Magn. Mater. 323 (2011) 1118–1127, http://dx.doi.org/10.1016/j.jmmm.2010.11.057.
[48] A.J. Rondinone, A.C.S. Samia, Z.J. Zhang, Superparamagnetic relaxation and magnetic anisotropy energy distribution in $CoFe_2O_4$ spinel ferrite nanocrystallites, J. Phys. Chem. B 103 (1999) 6876–6880, http://dx.doi.org/10.1021/jp9912307.
[49] C. Pereira, A.M. Pereira, C. Fernandes, M. Rocha, R. Mendes, M.P. Fernández-García, A. Guedes, P.B. Tavares, J.-M. Grenèche, J.P. Araújo, C. Freire, Superparamagnetic MFe_2O_4(M = Fe Co, Mn) nanoparticles: tuning the particle size and magnetic properties through a novel one-step coprecipitation route, Chem. Mater. 24 (2012) 1496–1504, http://dx.doi.org/10.1021/cm300301c.
[50] S.K. De, M. Krishna, Surendra, M.S. Ramachandra Rao, Application worthy SPIONs: coated magnetic nanoparticles, IEEE Trans. Magn. 50 (2014), http://dx.doi.org/10.1109/TMAG.2014.2305644.
[51] B. Bittova, J.P. Vejpravova, M.P. Del Morales, A.G. Roca, D. Niznansky, A. Mantlikova, Influence of aggregate coating on relaxations in the systems of iron oxide nanoparticles, Nano 7 (2012) 1250004, http://dx.doi.org/10.1142/s179329201250004x.
[52] K.C. Barick, S. Singh, D. Bahadur, M.A. Lawande, D.P. Patkar, P.A. Hassan, Carboxyl decorated Fe_3O_4 nanoparticles for MRI diagnosis and localized hyperthermia, J Colloid Interface Sci. 418 (2014) 120–125, http://dx.doi.org/10.1016/j.jcis.2013.11.076.
[53] G. Wang, S. Inturi, N.J. Serkova, S. Merkulov, K. McCrae, S.E. Russek, N.K. Banda, D. Simberg, High-relaxivity superparamagnetic iron oxide nanoworms with decreased immune recognition and long-circulating properties, ACS Nano 8 (2014) 12437–12449, http://dx.doi.org/10.1021/nn505126b.
[54] M. Estrader, A. Lopez-Ortega, S. Estrade, I.V. Golosovsky, G. Salazar-Alvarez, M. Vasilakaki, K.N. Trohidou, M. Varela, D.C. Stanley, M. Sinko, M.J. Pechan, D.J. Keavney, F. Peiro, S. Surinach, M.D. Baro, J. Nogues, Robust antiferromagnetic coupling in hard-soft bi-magnetic core/shell nanoparticles, Nat. Commun. 4 (2013) 1–8, http://dx.doi.org/10.1038/Ncomms3960.
[55] M. Mandal, S. Kundu, S.K. Ghosh, S. Panigrahi, T.K. Sau, S.M. Yusuf, T. Pal, Magnetite nanoparticles with tunable gold or silver shell, J. Colloid Interface Sci. 286 (2005) 187–194, http://dx.doi.org/10.1016/j.jcis.2005.01.013.
[56] R. Di Corato, A. Espinosa, L. Lartigue, M. Tharaud, S. Chat, T. Pellegrino, C. Menager, F. Gazeau, C. Wilhelm, Magnetic hyperthermia efficiency in the cellular environment for different nanoparticle designs, Biomaterials. 35 (2014) 6400–6411, http://dx.doi.org/10.1016/j.biomaterials.2014.04.036.